

---

## MEDICAL IMAGE AND INFORMATION PROCESSOR

**Michele Banish**

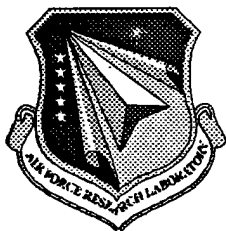
**SY Technology, Inc.  
654 Discovery Drive  
Huntsville, AL 35806**

**December 1999**

**Final Report**

APPROVED FOR PUBLIC RELEASE; DISTRIBUTION IS UNLIMITED

20000209 182



**AIR FORCE RESEARCH LABORATORY  
Directed Energy Directorate  
3550 Aberdeen Ave SE  
AIR FORCE MATERIEL COMMAND  
KIRTLAND AIR FORCE BASE, NM 87117-5776**

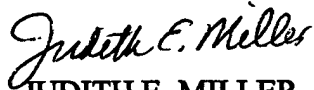
Using Government drawings, specifications, or other data included in this document for any purpose other than Government procurement does not in any way obligate the U.S. Government. The fact that the Government formulated or supplied the drawings, specifications, or other data, does not license the holder or any other person or corporation; or convey any rights or permission to manufacture, use, or sell any patented invention that may relate to them.

This report has been reviewed by the Public Affairs Office and is releasable to the National Technical Information Service (NTIS). At NTIS, it will be available to the general public, including foreign nationals.

If you change your address, wish to be removed from this mailing list, or your organization no longer employs the addressee, please notify AFRL/DEBA, 3550 Aberdeen Ave SE, Kirtland AFB, NM 87117-5776.

Do not return copies of this report unless contractual obligations or notice on a specific document requires its return.

This report has been approved for publication.



JUDITH E. MILLER, DR-2  
Project Manager

FOR THE COMMANDER



RICHARD J. BAGNELL, Lt Col, USAF  
Chief, ABL Technologies Branch



R. EARL GOOD, SES  
Director, Directed Energy Directorate

REPORT DOCUMENTATION PAGE			Form Approved OMB No. 074-0188	
Public reporting burden for this collection of information is estimated to average 1 hour per response, including the time for reviewing instructions, searching existing data sources, gathering and maintaining the data needed, and completing and reviewing this collection of information. Send comments regarding this burden estimate or any other aspect of this collection of information, including suggestions for reducing this burden to Washington Headquarters Services, Directorate for Information Operations and Reports, 1215 Jefferson Davis Highway, Suite 1204, Arlington, VA 22202-4302, and to the Office of Management and Budget, Paperwork Reduction Project (0704-0188), Washington, DC 20503				
1. AGENCY USE ONLY (Leave blank)	2. REPORT DATE December 1999	3. REPORT TYPE AND DATES COVERED Final Report 20 Dec 95- 1 Dec 99		
4. TITLE AND SUBTITLE Medical Image and Information Processor		5. FUNDING NUMBERS C: F29601-96-C-0015 PE: 65502F PR: 3005, TA: C0, WU: LE		
6. AUTHOR(S) Michele Banish				
7. PERFORMING ORGANIZATION NAME(S) AND ADDRESS(ES)  SY Technology, Inc. 654 Discovery Drive Huntsville, AL 35806		8. PERFORMING ORGANIZATION REPORT NUMBER		
9. SPONSORING / MONITORING AGENCY NAME(S) AND ADDRESS(ES)  Air Force Research Laboratory Directed Energy Directorate/Airborne Laser Technology Branch (AFRL/DEBA) 3550 Aberdeen SE Kirtland AFB NM 87117-5776		10. SPONSORING / MONITORING AGENCY REPORT NUMBER AFRL-DE-TR-1999-1032		
11. SUPPLEMENTARY NOTES				
12a. DISTRIBUTION / AVAILABILITY STATEMENT Approved for Public Release; Distribution Unlimited			12b. DISTRIBUTION CODE	
13. ABSTRACT (Maximum 200 Words) Pulse Coupled Neural Networks (PCNN) have been extended and modified to suit medical image segmentation applications. Previous research demonstrated the ability of a PCNN to ignore noisy variations in intensity and small spatial discontinuities in images that prove beneficial to image segmentation and image smoothing. This final report describes three research and development projects that relate to PCNN segmentation - three different digital image processing applications and a CMOS integrated circuit implementation. The software for the diagnosis of Pulmonary Embolism from VQ lung scans uses PCNN in single burst mode for segmenting perfusion and ventilation images. The second project is attempting to detect cardiac infarct and ischemia by comparing 3-D SPECT (Single Photon Emission Computed Tomography) images of the heart obtained during stress and rest conditions, respectively. The third application is a study of the full body bone scans for the detection of cancer. This paper also describes the hardware implementation of PCNN algorithm as an electro-optical chip.				
14. SUBJECT TERMS Pulse coupled neural networks, image segmentation, cancer, pulmonary embolism, ischemia, image segmentation			15. NUMBER OF PAGES 38	
			16. PRICE CODE	
17. SECURITY CLASSIFICATION OF REPORT Unclassified	18. SECURITY CLASSIFICATION OF THIS PAGE Unclassified	19. SECURITY CLASSIFICATION OF ABSTRACT Unclassified	20. LIMITATION OF ABSTRACT Unlimited	



## Table Of Contents

Table Of Contents .....	iii
Figures.....	iv
Tables .....	v
Summary .....	vi
Introduction.....	1
Detection of Pulmonary Embolism .....	2
Detection of Infarction and Ischemia .....	5
Location of Bone Cancer in Full Body Bone Scans.....	6
Hardware Architecture Pulse Coupled Neural Network Chip.....	8
Methods, Assumptions, and Procedures.....	9
Basis Lung Scan Interpretation Algorithm.....	12
Basis of Cardiac Scan Algorithm .....	18
Basis for Bone Scan Interpretation Algorithm .....	18
Results and Discussion.....	20
Why use a Pulse Coupled Neural Network .....	23
Hardware Implementation of the Pulse Coupled Neural Network .....	23
Recommendations .....	27
References .....	28

## Figures

Figure	Page
1.) a). Normal VQ scan b). abnormal VQ scan. The first row shows ventilation images and other rows show perfusion images.	4
2.) Two perfusion scans: The box shows overlapped left and right lungs. Arrows point to areas of low perfusion.	5
3.) Cardiac SPECT imagery. Raw data - rows one and two; PCNN output-rows five and six; cleaned, enlarged images with defects marked-rows three and four.	6
4.) SPECT bone scan image. A physician has marked ROIs by drawing circles. The PCNN locates the same ROI and marked it with an outlined area and filled in an area in red. c) In a second patient scan the PCNN locates many cancerous lesions as ROIs.	7
5.) Optical input PCNN Chip.	9
6.) Each posterior lung is divided into two regions: lateral and medial. Each region is then subdivided into an upper, middle or lower region.	12
7.) Concave defects at the edge of the lung are detected and their position and size are recorded.	13
8.) Lungs and the a) successful and b) unsuccessful segmentation results	14
9.) A Perfusion lung that fragments into small contiguous areas rather than one lung. The gaps denote significant defects.	16
10.) Examples of perfusion lungs that differ in size from the ventilation lungs. In this case the left perfusion lung is also smaller than the right lung	16
11.) Undetected wedge shaped defect (lingula) located near white arrows.	21
12.) Pulse coupled neuron schematic. This neuron is one pixel. The lightning bolt arrow is the optical input. This input can be overridden in an electronic PCNN also under development. b) The L-Edit layout for the pixel/neuron. c) tiled 32x32 PCNN array.	25
13.) Segmented image with $\frac{1}{2}$ of array illuminated .	26

## Tables

Table	Page
1. Lung Scan Interpretation using PCNN Segmentation	4
2 PCNN Prototype Test Result	26

## Summary

Pulse Coupled Neural Networks (PCNN) have been extended and modified to suit medical image segmentation applications. Previous research demonstrated the ability of a PCNN to ignore noisy variations in intensity and small spatial discontinuities in images that prove beneficial to image segmentation and image smoothing. This final report describes three research and development projects that relate to PCNN segmentation - three different digital image processing applications and a CMOS integrated circuit implementation. The software for the diagnosis of Pulmonary Embolism from VQ lung scans uses PCNN in single burst mode for segmenting perfusion and ventilation images. The second project is attempting to detect cardiac infarct and ischemia by comparing 3-D SPECT (Single Photon Emission Computed Tomography) images of the heart obtained during stress and rest conditions, respectively. The third application of the PCNN in full body bone scans for the detection of cancer. This research transitioned military PCNN technology to demonstrate and test algorithms that automate image interpretation. Test results were obtained from a blind clinical trial and the algorithm categorized the patients based on the quantitative analysis of the medical images physicians review.

These applications were used to develop requirements for the hardware implementation of the PCNN. Two PCNN hardware versions are under development. One operates with electronic input and the second chip operated with an optical input. The electronic input PCNN is still in the design and modeling stage. The experience gained in developing prototype chip confirms that PCNN can be implemented as integrated circuit at reasonable cost. Further testing and study is needed to fully understand and validate the chip's performance. Availability of a full array will benefit real time processing of images. Market opportunities exist for a general prototype suitable for experimentation and also specialized chips for specific applications.



## Introduction

Advances in artificial neural networks that emulate biological systems have been used for digital image processing. However, most artificial neuron models fail to capture functional complexities of their biological counterparts. This is one reason for the limited success of artificial neural networks in the domain of image processing. Achieving the functional complexities needed to address image processing through network size and topology seems unsolvable without improving the neuron model. Recently significant progress has been made toward the development of neuron models that resemble the cortical neuron.

*Eckhorn* [1990] performed experimental studies of a cat's visual cortex, and developed a neuron model that captures some of the salient cortical neuron features. Eckhorn's model and its variants are referred to as pulse coupled neurons (PCN) and neural networks which use pulse coupled neurons are called pulse coupled neural networks (PCNN). *Ranganath et al.* [1994] significantly altered the pulse coupled neuron model to optimize its function in image processing applications. This pulse coupled neural network functions in a manner that is beneficial to image segmentation and image smoothing.

*Kuntimad* [1995] studied the segmentation capability of the PCNN and compared its performance with several commonly used methods ( relaxation approach, optimum thresholding, region growing methods ). In general, an image is segmented by PCNN by adjusting the values of two network parameters such that neurons corresponding to pixels of a region pulse together and groups of neurons corresponding to adjacent regions pulse at different times. The two network parameters are the linking coefficient and the radius of the linking receptive field. If an image consists of two regions, object and background, PCNN may be used in a single burst mode to separate object pixels from the background pixels. When intensity ranges of two regions overlap, no thresholding method is able to perfectly separate one region from the other. However, depending on the extent of overlap, the PCNN is capable of producing such a perfect segmentation result. Conditions for perfect segmentation of two region images are derived by *Kuntimad* [1995]. When the two intensity levels overlap extensively, even though perfect

segmentation is not possible, the PCNN performs remarkably well. When the image consists of more than two types of regions, the PCNN may be used in multiple burst mode. Kuntimad [1995] has developed a knowledge-based system in which PCNN is used in multiple burst mode to segment complex images iteratively. Each iteration improves the result of the previous iteration by updating network parameters. Three medical software applications and a PCNN opto-electronic integrated circuit implementation of the PCNN are discussed.

### Detection of Pulmonary Embolism

Valdivia [1997] writes that pulmonary embolism is a medical condition associated with approximately 250,000 hospitalizations and 50,000 deaths annually in the United States. However, less than 10% of patients are treated for the condition because of the difficulties encountered during diagnosis. Medical doctors use VQ scans to infer or detect pulmonary embolism. A VQ scan image set consists of 8 digitally acquired perfusion images and more than 40 digitally acquired ventilation images of the lungs. Perfusion images monitor carbon dioxide/oxygen exchange at the lung exterior and the ventilation images monitor the oxygen/carbon dioxide exchange on the inside of the lung. The diagnostic data is diminished intensity or voids that are useful in identifying lung regions that do not receive sufficient blood to support the gas exchange. These perfusion images are taken in rotational intervals of 45 deg. All ventilation images cover the same posterior view of the lungs and are taken over a period of several minutes at regular time intervals of 30 secs. These images are plagued by poor contrast and low signal to noise ratio, figure 1.

At present doctors interpret VQ scans visually, looking for intensity voids and hot spots. They classify the patient into pulmonary embolism categories: *high*, *low* or *intermediate*. The scans assigned to the *intermediate* category mean the patient may or may not have PE and must undergo further testing to confirm or rule out the condition. Obviously an intermediate diagnosis is not useful. The next test is pulmonary angiography, a relatively expensive test that has high morbidity and mortality rates associated with it. The poor data quality and subjectivity of the interpretation causes a lot of inconsistency in VQ scan interpretations.

The physician's software tool for the detection of pulmonary embolism uses PCNN in single burst mode to segment perfusion and ventilation images. In each image, PCNN identifies the group of pixels that form the left and right lungs. The parameter values (linking coefficient and initial threshold) are derived from input images without user intervention. All neurons with primary input greater than the initial threshold fire naturally and use linking signals to capture neighboring neurons in a recursive manner. Since the threshold signal generator is eliminated the network operates quickly. Regions of low perfusion do not pulse with other lung regions and appear as holes or concave defects in segmented images.

In a blind FDA clinical study performed at the University of Utah Medical School, the PCNN based Lung Scan Interpretation tool was used to perform fully automated computer diagnosis of patients that were candidates for acute pulmonary embolism. One hundred and three consecutive ventilation /perfusion (VQ) lung scans for acute pulmonary embolism (PE) were studied. Three nuclear medicine physicians interpreted the VQ scans using the currently approved diagnostic rules outlined in the NIH PIOPED study. The computer program used the PCNN to identify the lung and identify concave defects along the lung periphery. This criterion for diagnosis is akin to the rules outlined in the PIOPED logic was used to correlate ventilation and perfusion defects and assign a score of low, intermediate, or high probability for PE. The computer interpretations were then compared to the interpretations of the physicians. The clinical follow-up of all patients at six months consisted of medical record review for the results of pulmonary angiography, chest CT, extremity doppler ultrasound, and repeat lung scans. Sufficient clinical data for 81 patients was collected and analyzed in this evaluation. The diagnosis was confirmed by a review of patient records during a six month follow-up, table 1.

The computer software correctly diagnosed 70 of 81 (86%) VQ scans. There were two false negative studies (normal or low probability patients with PE) and four false positive studies (high probability without PE). The computer classified only five scans to the intermediate category. In comparison, the physician interpretation was correct in nine of 15 patients with PE and 39 of 66 patients without PE. The physicians interpreted 40% of the studies as intermediate

while the computer interpreted only 6% as intermediate. In order to achieve these results, the PCNN algorithm was used to separate overlapping lungs as shown in figure 2. The first pass of the PCNN located the boundary incorrectly. Iterative processing with varying beta produced the correct segmentation result. The lingula (small segmental defect) was successfully located by the PCNN based software.

Table 1. Lung Scan Interpretation using PCNN Segmentation

Diagnosis	15 Patients with PE		66 Patients without PE	
	Physicians	Computer	Physicians	Computer
High	9	13	0	4
Intermediate	5	0	27	5
Low	1	2	36	39
Normal	0	0	3	18

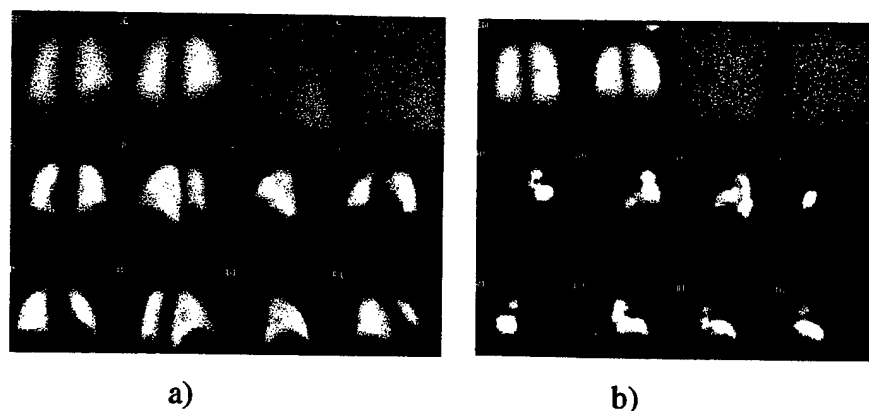


Figure 1: a) Normal VQ scan b) abnormal VQ scan. The first row shows ventillation images and other rows show perfusion images.

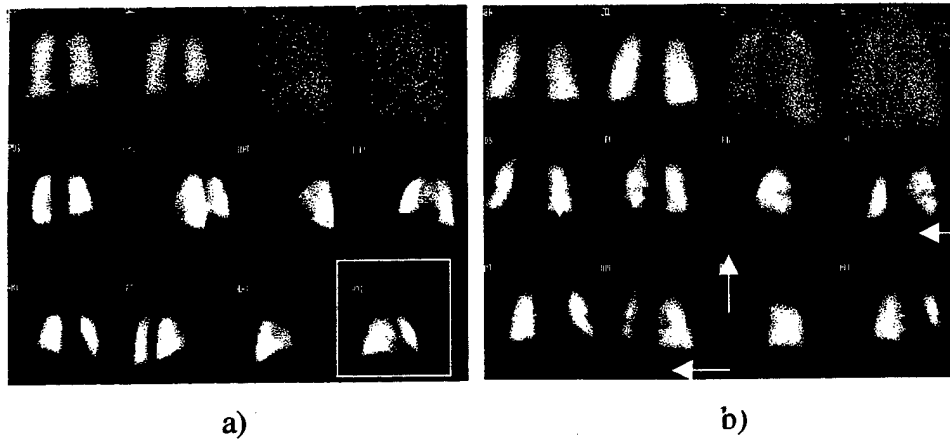


Figure 2. Two perfusion scans: a) The box shows overlapped left and right lungs. b) Arrows point to areas of low perfusion.

### Detection of Infarction and Ischemia

Cardiac disease, infarct and ischemia, can be diagnosed with a cardiac Single Photon Emission Computed Tomography (SPECT) study. This data set is digital and provides a three-dimensional reconstruction of the myocardium at rest and during stress. Physicians view the study as slices of the heart made in three directions, horizontal short axis, vertical and horizontal long axes. The physicians select planes through the reconstructed heart and interactively examine myocardial activity. Various radionuclides such as thallium-201 are used to improve image quality. Due to superior diagnostic property over planar images, SPECT images also allow for the quantitative analysis heart's functionality. Ranganath and Banish are developing a software tool to assist physicians when they screen patients for ischemia and infarction. The software compares the imagery obtained during exercise (stress profile) with the imagery obtained during rest (rest profile). Regions with reduced perfusion in stress profile in comparison with the perfusion in rest profile indicate ischemia. Regions with reduced perfusion in both profiles usually indicate infarction. The software has to handle blurring due to motion, hot spots, noise and variation due to anatomical structure of patients. Early study shows that PCNN is able to detect regions that indicate ischemia or infarction. The neural network has consistently separated pixels of reduced perfusion from normal pixels under various imaging conditions. It has also succeeded in cleaning unwanted clutter around myocardium and suppressing hot spots. At present the software has correctly interpreted 39 of a total of 42 data sets tried. Sample cardiac imagery is

shown in figure 3. The first two rows of data show a partial set of the raw SPECT slices along the short axis. Row one is taken during stress and row two is taken during rest. Row five and six are obtained by enlarging the segmented images. Rows three and four display segmented images in their original intensity along with arrows pointing to defects.

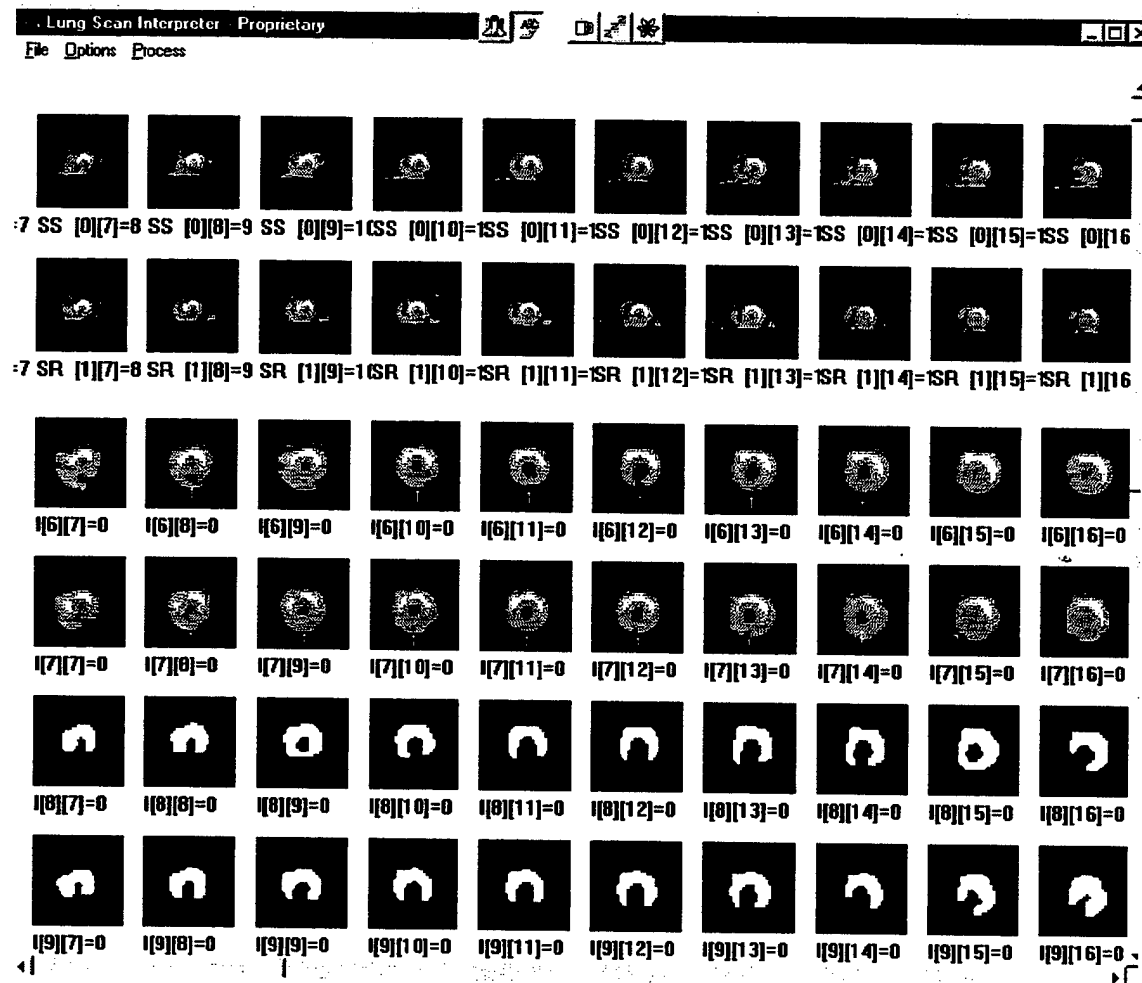


Figure 3. Cardiac SPECT imagery. Raw data - rows one and two; PCNN output - rows five and six; cleaned , enlarged images with defects marked - rows three and four.

### Location of Bone Cancer in Full Body Bone Scans

To illustrate another medical region of interest application, Figure 4a shows a full body SPECT bone scan. This scan is made to diagnose a host of diseases, one of which is bone cancer. The

data is very noisy and therefore diagnostic features can be subtle. Noise is caused by the acquisition protocol, patient motion, patient body mass and marker uptake variability. In Figure 4b, the upper torso of a man with cancer is shown. Cancerous lesions in the upper torso have been identified in full bony bone scans. These appear as bright spots on bones. However, not all bright spots are lesions. The PCNN based region evaluation module sorts cancerous lesions from hot spots associated with arthritis. The two measures used to locate true lesions from non-cancerous areas were mean and standard deviation of the automatically selected region. Cancerous lesions are local peaks, as in the correlation surface automated target applications. Figure 4c shows many regions of interest (red areas) overlaid onto the original torso intensity. These regions need to be ranked because there are true and false lesions among the PCNN segmentation results. The segmentation results are referred to as regions of interest (ROI).

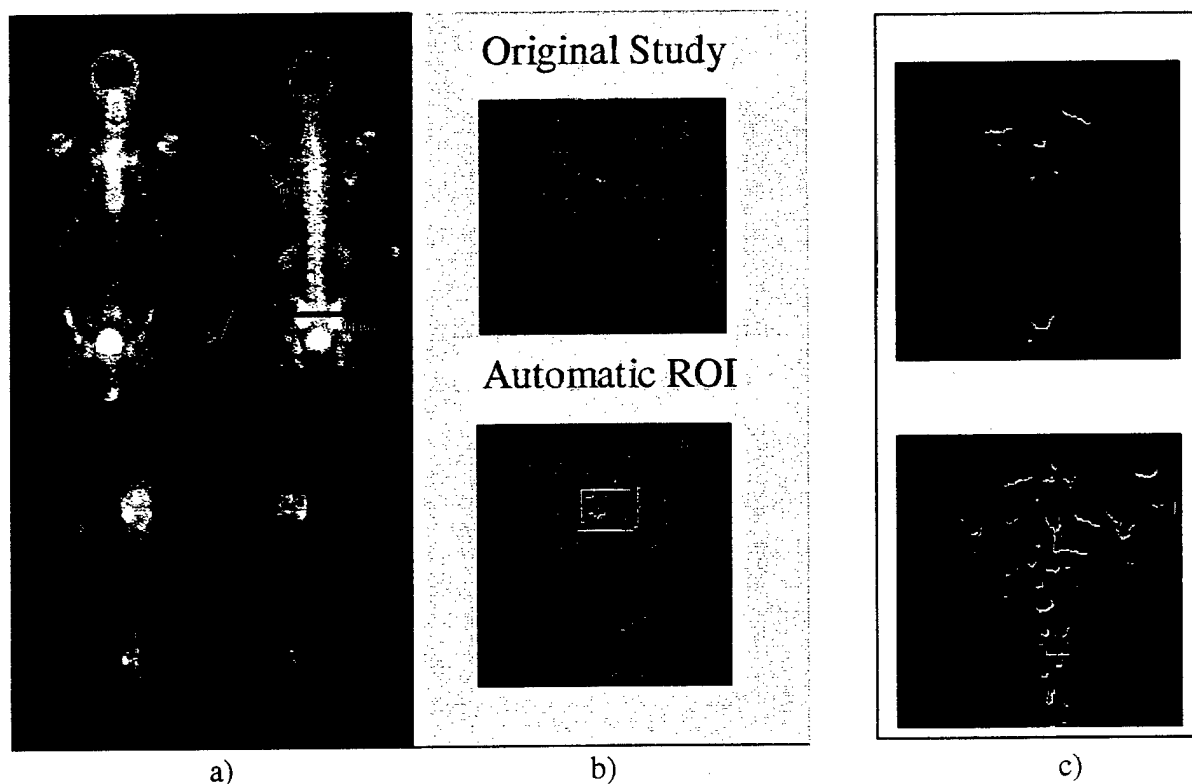


Figure 4. a) SPECT bone scan image. A physician has marked ROIs by drawing circles. b) The PCNN locates the same ROI and marked it with an outlined area and filled in an area in red. c) In a second patient scan, the PCNN locates many cancerous lesions as ROIs.

## Hardware Architecture Pulse Coupled Neural Network Chip

One practical issue in applying the PCNN algorithm is the processing speed. The PCNN based image segmentation systems are expected to deal with a large number of two-dimensional images and also three-dimensional images. Therefore, to process images in real or near real time, a PCNN must be implemented as a fast hardware circuit with externally controllable parameters. SY Technology and its commercial subsidiary MemsOptical Inc. have designed and fabricated one such chip. Even though full design details are intentionally left out, the readers will get a fair idea about the capabilities of the PCNN integrated circuit.

An 11 x 11 PCNN prototype chip has been fabricated. The size of the chip is 2 mm x 2 mm square and spacing between neurons is 122  $\mu\text{m}$ . It is fabricated on the HP 0.5  $\mu\text{m}$  process offered by the MOSIS foundry service. The external or primary input to each neuron is optical. A photodiode converts light to a voltage. A lenslet array covers each neuron, and an imaging lens assists the imaging of light onto the chip, so it acts like a camera. Each neuron is linked to all other neurons in the network by a grid of resistors. The linking coefficient and threshold signal are global parameters and input externally.

The chip uses multiplexed outputs, each neuron is addressed by its row and column location. The addressing scheme is same as that used in CCD cameras. The chip outputs a binary image at each threshold indicating the neurons fired. We have used a linearly decaying threshold signal in our design.

A photodiode (lower left figure 5) is light sensitive, and feeds an amplifier and multiplier circuit. The linking and optical input are summed and compared to a threshold voltage. This internal activity value is above the current threshold the neuron fires. The chip outputs a binary image at each threshold level. Firing neurons are high and non-firing neurons are low.



## 1 Pixel/Neuron Circuit

## PCNN Pixel

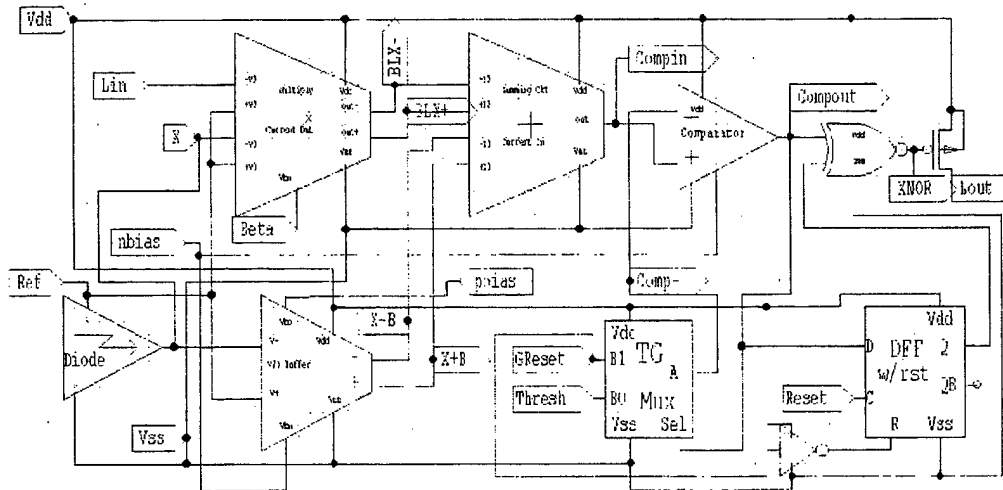


Figure 5. Optical Input PCNN Chip.

The 11 x 11 array is an experimental prototype, from which larger arrays will be based. Several pins provide observation points for various signals within the circuit. The prototype is still in the debugging phase. Several prototypes of the 11 x 11 have been made in order to understand and optimize the chip's performance in the above mentioned applications. Test data is being accumulated to demonstrate the performance of the chip. This data will then be compared to the results of the circuit simulation to validate the circuit operation. To better facilitate chip design a functional electronic model has been developed.

## Methods, Assumptions, and Procedures

Computer-aided interpretation of diagnostic images is a subject of considerable interest in many areas of medicine including nuclear medicine, radiology, echo cardiology and magnetic resonance imaging. Image processing and pattern recognition methods which are successfully used to solve many diverse and challenging problems, if adapted and applied properly, can provide many useful clinical decision support tools for physicians.

For example, the diagnosis of acute PE is difficult due to the low sensitivity and specificity of the clinical signs and symptoms. VQ scans are noninvasive tests that give the probability of PE for a given patient. Unfortunately a large number of scans, 39%(1), fall into the intermediate probability group. Although an experienced reader has a high accuracy rate just using "gestalt" (2), the less experienced reader must rely on various criteria for interpretation. These interpretation schemes are not standardized. In addition there is significant interobserver variability, particularly in the low and intermediate probability categories (3). This paper describes a fully automated computer program that aids the nuclear medicine physician to interpret VQ scans and categorize the probability of PE as high, low or intermediate. Some of the salient features of the VQ scan interpretation software are given below:

1. The software alerts the reader when images have poor count density and are not suitable for reading.
2. The software enhances ventilation and perfusion images for better human perception.
3. All significant defects are ranked, marked and displayed on the monitor for physician's review.
4. The program generates a detailed report that includes clinical and quantitative description of defects and the decision logic used for the final classification of PE.
5. The study shows that the software significantly reduces the percentage of scans assigned to the intermediate category without compromising accuracy.

In each study (lung, cardiac and bone) a patient population who had undergone the appropriate scans for acute disease were included in the study. In each study, the scans were interpreted by physicians, according to the appropriate medical criteria, by three nuclear medicine physicians. All potential defects were identified with the help of the artificial neural network known as pulse coupled neural network. Regions of interest were located and evaluated through quantitative analysis of each image sequence. Based on quantitative attributes of each type of defect, matching relevant images with one another, defects were ranked as large, medium, small and insignificant. Based on the number of defects and their severity, software assigned a probability of **high, intermediate** or **low** for the specific disease. In the case of the lung study, a six month follow up of all patients consisted of medical record review of pulmonary angiography, chest CT, extremity doppler US, and repeat lung scans. The final diagnosis for

pulmonary was confirmed by patient records and the performance of the software tool was then compared with those of physicians. In the case of the other studies, agreement among by three physicians was considered the gold standard (truth).

The lung code is the basis for both other algorithms, in fact, the lung code has been applied to mine detection, ultraviolet satellite imagery, and automated target recognition correlation surfaces. Once data is processed through the lung code, the small details of detection are fine tuned to be specific to the data set. For example, the initial version of the lung software resulted in six false negatives (patients without the disease classified as high probability) and eighteen false positives (patients with the disease classified as low probability). Based on the analysis of these results several improvements were made to the detection algorithm. Usually it is the case that it is just the segmented region algorithm that requires fine-tuning. In this lung case, methods for improved defect detection and classification included better separation of left and right lungs in oblique views, improved recognition of effects of heart in anterior views and diaphragms in lateral views. These enhancements decreased the number of false negative and false positive studies to one and zero, respectively. In comparison, physicians also had one false negative study. However, physicians classified 33% of the studies as intermediate while the software interpreted only 5% as intermediate.

The study protocol included a population of 103 patients who had undergone VQ scans for acute PE. A population of 80 patients who had undergone full body scans for acute bone cancer were included in the bone study. A population of 40 patients who had undergone cardiac scans for infarct and ischemia were included in the cardiac study. Lung scans consisted of a posterior ventilation study performed using 370-555 MBq Xe-133, followed by an eight view perfusion study using 111-185 MBq TC-99m MAA containing approximately 200,000 to 500, 000 particles. Each perfusion lung image is a 256X256 array of pixels and each ventilation lung image is a 128x128 array of pixels. Cardiac data is 64x64 and the bone scans are 256x1024. The radionuclide imaging protocol for cardiac including sestamibi and thallium. The bone scan protocol was not available at the time of the preparation of this report. In all three studies, the pixel intensity is stored as a 16-bit unsigned number.

## Basis Lung Scan Interpretation Algorithm

A step by step description of the VQ lung scan interpretation algorithm is given in this section.

**Step 1:** The ventilation image sequence is processed to determine regions of strong and moderate retention.

- a. Seven ventilation images at the end of the washout sequence are added form IM.
- b. The first two images in the ventilation sequence (single breadth and equilibrium images) are analyzed and the one with better intensity count and homogeneity is selected as the reference Ventilation image for matching with perfusion images later during the analysis. If both images unsatisfactory due to poor inhalation, the user is warned of poor quality ventilation images and then proceeds with the analysis. In this case the diagnosis may not be reliable.
- c. The image selected in step 1b is processed using PCNN and regions corresponding to left and right lungs are determined. The PCNN produces a binary image in which lung and background pixels are bright and dark, respectively.
- d. Each lung is divided into six regions as shown in figure 6. Each region is classified as a region of high, moderate, mild or insignificant retention by comparing regions' average intensity with the average intensity of the same region in IM.

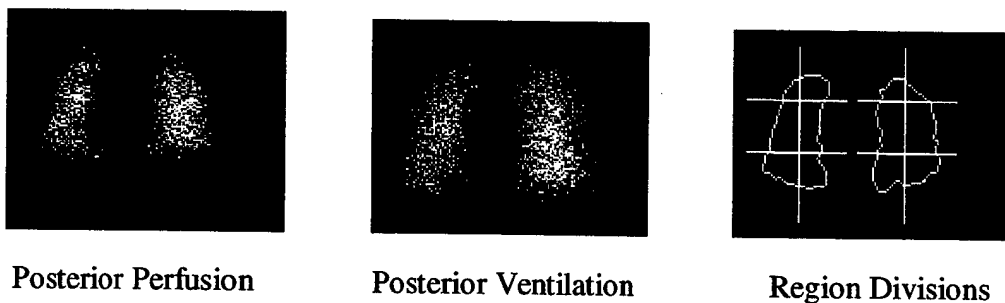


Figure 6. Each posterior lung is divided into two regions: lateral and medial. Each region is then subdivided into an upper, middle or lower region.

**Step 2:** The boundary of each lung as defined by the binary ventilation image is extracted and stored using eight way chain code. For each lung, several geometric attributes are computed.

These include size, perimeter, height and width of the lung and erosion in the medial, basal, apical and lateral regions.

**Step 3:** The binary ventilation image is also used to find defects or parts of lungs with diminished radionuclide concentration. In ventilation image, pixels that belong to the lung are usually brighter than non-lung pixels. However, defective lung segments, if any, appear much darker than normal lung segments. As a result these darker lung segments usually blend with the background when processed by the PCNN. Therefore, the segmentation of the ventilation image using the PCNN may lead to any of the following results:

- a. A lung with very large defects near the base or apex appears small in size in the binary image. This is because a large number lung pixels blend with the background.
- b. Some long and narrow defects may cause a lung to appear fragmented in the binary image.
- c. Interior defects appear as holes and peripheral defects appear as concavities along the boundary of the lung. Position and size of each such defect are determined and stored, figure 7.
- d. If there are no ventilation defects then none of the above are true.

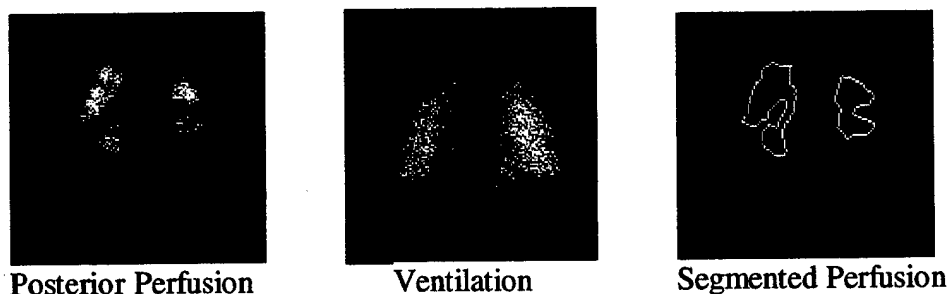


Figure 7. Concave defects at the edge of the lung are detected and their position and size are recorded.

**Step 4:** Each of the eight perfusion images are processed to determine all potential perfusion defects and their attributes.

- a. The image is smoothed using a neighborhood averaging method to reduce the ill effects of random noise. Any lowpass filter can be used for this purpose.

- b. The smoothed image is applied as input to the PCNN and segmented to produce the bilevel image in which lung and non-lung pixels are set to 255 and 0, respectively.
- c. A region-growing algorithm is used to determine all the regions present in the image. Ideally each lung must appear as one connected region. However, this may not be true due to the reasons described in step 3. The boundary of each region is stored using eight-way chain code.
- d. All regions that belong to left lung are identified. Similarly, all regions that belong to right lung are also identified.
- e. Size and position of all defects that appear as interior holes and concavities along the lung boundary are determined. Each defect is classified as large, medium, small and insignificant based on size, location and depth. For example, a lateral defect is more significant than a medial defect of equal size.
- f. Basal, apical, medial and lateral erosions are computed for left and right lungs for posterior and anterior views.
- g. The pulse coupled neural network may not always succeed in separating left lung from right lung while processing oblique views. This is especially true for images that represent anterior oblique views. A procedure has been developed to separate left lung from right lung if the PCNN fails to do so, figure 8.

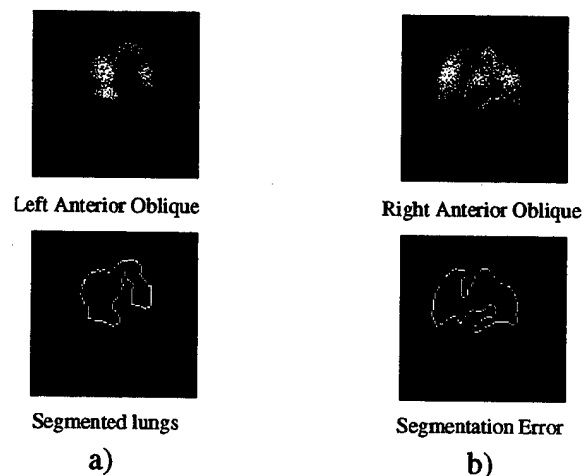


Figure 8. Lungs and the a) successful and b) unsuccessful segmentation results

- h. In lateral views, only one lung is visible. Also, the diaphragm may look like a concave defect. Therefore, defects in this area are further analyzed based on depth and curvature of the concavity. It is taken as a valid defect only if certain specified constraints are satisfied.

**Step 5:** In this step redundant defects and unsupported medial defects are deleted. If two defects appear very close to each other then the smaller defect is considered as redundant and deleted. An unsupported medial defect is visible in only one view and is not considered significant unless it is large.

**Step 6:** It is possible that a defect may appear or visible in more than one view. All instances of the each defect are identified and tagged.

**Step 7:** Perfusion defects in posterior view are matched or correlated with ventilation defects. All perfusion defects that have matching ventilation defects are tagged and deleted from further consideration.

**Step 8:** In this step perfusion defects are deleted or downgraded based on retention in ventilation lungs. If strong retention is detected in the region of the lung that corresponds to the position of the defect, the defect is not included in the decision making process. If the retention is moderate the defect is downgraded by one step (large to medium, medium to small, small to insignificant).

**Step 9:** Based on the number of defects, their attributes and quantitative measures of erosion (blunting), final diagnosis is made. The software assigns high probability for PE if one or more of the following conditions are true and stops. Otherwise, the program proceeds to step 10.

- a. Only one lung is detected by the PCNN in the posterior or anterior perfusion view when both lungs are clearly visible in the ventilation image. This covers the cases in which diminished radionuclide concentration is obvious in most of the lung's segments.

- b. Left or right perfusion lung appears fragmented in the binary images produced by the PCNN and ventilation lungs to not appear fragmented, figure 9.
- c. The size of one of the perfusion lungs in posterior or anterior view is much smaller than the other lung as compared to the relative sizes of ventilation lungs, and excessive erosion is observed in the basal or apical region of the smaller perfusion lung, figure 10.
- d. One or more large unmatched defects exist in a perfusion lung and no defects or retention is detected in the corresponding ventilation lung.

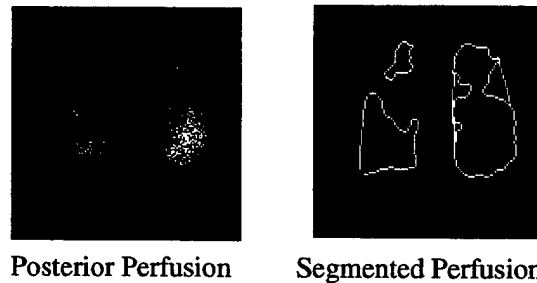


Figure 9. A perfusion lung that fragments into small contiguous areas rather than one lung. The gaps denote significant defects.

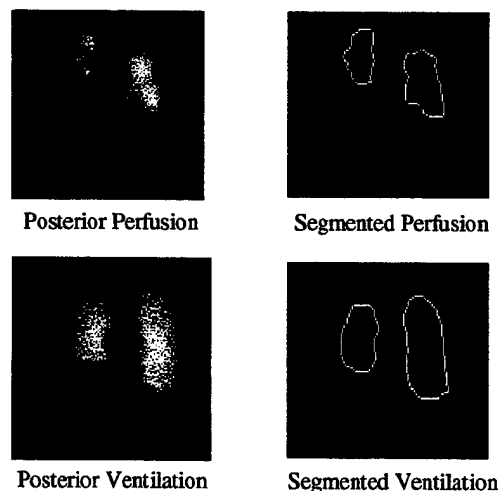


Figure 10. Examples of perfusion lungs that differ in size from the ventilation lungs are shown. In this case, the left perfusion lung is also smaller than the right lung.



**Step 10:** If the probability of PE is not found to be high in step 9, the left and right ventilation lungs are ranked as good or bad. A ventilation lung is ranked as bad if any one of the following conditions is true.

- a. If one or more large defects are present.
- b. The number of large and medium defects in the lung is greater than two.
- c. The lung fragments when segmented by the pulse coupled neural network.

**Step 11:** If left ventilation lung is classified as good in step 10, left lung is examined for the presence of a lateral defect and medial defect (small or medium), approximately in the middle third of the lung with a band of slightly darker pixels connecting them. If such defects and pixel band are found the probability of PE is assigned the value high.

**Step 12:** If the probability of PE is not found to be high in previous steps and if one or more of the following conditions are true the scan is assigned to the intermediate probability category.

- a. One perfusion lung in posterior view is significantly smaller than the other in comparison with the relative sizes of ventilation lungs and there is no significant apical or basal erosion.
- b. A lung which is ranked as good in the ventilation image has three or more small and medium unmatched perfusion defects.
- c. A lung that is ranked as bad in the ventilation image has six or more unmatched perfusion defects.
- d. The ratio of medial erosion to area of a lung in posterior perfusion image is greater than 0.3 and also greater than twice the ratio of medial erosion to lung area of the lung in posterior ventilation image.
- e. Intensity analysis reveals that a region whose area is greater than 30% of the area is darker than the rest of the lung. Only those pixels of the input image which are identified as lung pixels by binary perfusion images are used for area computation and intensity analysis.

**Step 13:** If the probability of PE is not high or intermediate then it must be low. If both ventilation lungs are ranked as good and no defects are found in perfusion images, the lungs are called normal.

### Basis of Cardiac Scan Algorithm

A step by step description of the cardiac scan interpretation algorithm is given in this section.

**Step 1:** The cardiac scan image short axis planar image sequence is processed to determine regions of the myocardium.

- a. rest images are segmented
- b. stress images are segmented

**Step 2:** The boundary of each heart as defined by the binary image is extracted and stored using eight way chain code. For each heart, several geometric attributes are computed. These include any deviation from the normal circumference of a heart.

**Step 3:** If a concavity is located in the external contour it is a cardiac defect.

**Step 4:** If the location of a concavity matches between the stress and rest imagery, then the diagnosis is infarct. If there is a stress defect and no rest defect at a location then it is a diagnosis of ischemia.

### Basis for Bone Scan Interpretation Algorithm

In the process for determining which patients had cancer and which did not, an image registration algorithm was developed. In accordance with customary protocol, we are including the pseudocode for that algorithm here. Once registered, the PCNN performs region of interest location via the same single pass segmentation scheme as described above.

Pseudocode for Image registration (ref - Phase I final report SYT95-TR-085)

```
/* genetic algorithm mapping algorithm */  
Initialize candidate mappings (random draws)
```

```

for( max iterations){
    evaluate candidate mappings
    mutate candidate mappings
    micro genetic algorithm loop{
        while(not converged){
            evaluate and rank candidate mappings
            regenerate population{
                save best mapping
                combine the best and third best mappings
                combine the second and fourth best mappings
            }
        }
    }
}

```

*/\* lesion detection algorithm \*/*

*compute mean image*

*compute variance image*

*PCNN segments regions with potential regions above reference threshold*

*determine texture of points exceeding threshold*

*Initialize candidate mappings* - five candidate solutions are initialized using random draws from a uniform distribution. The range of mappings are such that the control points are fixed to individual domains not overlapping.

*evaluate candidate mappings* - after the mappings are established, they are evaluated with the Mean Squared Error (MSE) with the desired image region. However, before this is accomplished, a smoothing kernel is convolved with the mapped image. This smoothing removes any voids created in the stretching of the image.

*mutate candidate mappings* - once a good estimate is obtained, the remaining four mapping estimates are created with randomized mutations of the good estimate. This randomization is adaptively updated to fine-tune the solution in later iterations.

*micro genetic algorithm loop* - this is the micro genetic algorithm control structure. In this loop, numerous cycles are performed until the MSE's of the individual estimates are all equal to within a numerical error constant. Typically, this will be performed in 10 to 30 iterations.

*evaluate and rank candidate mappings* - evaluation is performed on candidate mappings using the MSE functional previously defined. After the evaluation, the five candidates are ranked from the best to the worst, i.e. 1 thru 5. This ranking is then used to select which estimates are combined to form new ones in the next iteration.

*save best mapping* - the best estimate is retained for the next iteration. This process is termed "elitism" and has been demonstrated as a key feature in determination of an optimal mapping.

*combine the best and third best mapping* - the best and third best mapping candidates are uniformly combined to create two new candidate mappings. It is important to note that combining two estimates which are ranked next to each other causes premature convergence in the population of mappings. To circumvent this, alternate pairs are combined, i.e. 1 with 3, and 2 with 5.

A step by step description of the bone scan interpretation algorithm is given in this section.

**Step 1:** The bone scan image is processed to determine regions of high radioactivity.

**Step 2:** The location of the regions of interest are matched to typical signals from a reference body. The reference body was used during the image registration process.

**Step 3:** If the location of a concavity matches between the reference and patient imagery, then the diagnosis is not cancer. If there is a mismatch between the region of interest and the reference region, the diagnosis is cancer.

## Results and Discussion

The first software package developed was a medical application was lung scan diagnosis. A set of 70 VQ scans provided by the University of Utah medical center, Salt Lake City, were used as

examples to develop this lung software. After extensive discussions with two nuclear medicine physicians, the first version of the software was developed. As mentioned earlier a set of 103 VQ scans were then used for testing the software. The software called six scans normal or assigned low probability for PE while angiograms confirmed PE. Also, eighteen scans were incorrectly called high. In short, the first version resulted in six false negatives and eighteen false positives.

After reviewing those false negative and false positive patients, physicians identified the following five problems caused the false positives and false negatives.

- 1) In some cases, while processing oblique views (mostly in anterior oblique views), the PCNN was not able to separate left and right lungs completely. As a result, the analysis algorithm detected large concave defect in the region where the two lungs join and incorrectly assigned high probability for PE.
- 2) The shadow of the heart visible in anterior view was treated as a defect by the software when the heart was large.
- 3) The normal diaphragmatic contours in lateral views were sometimes taken as concave defects.
- 4) The software was unable to detect wedge shaped defects that appear as medial defects in posterior and anterior views, figure 11.

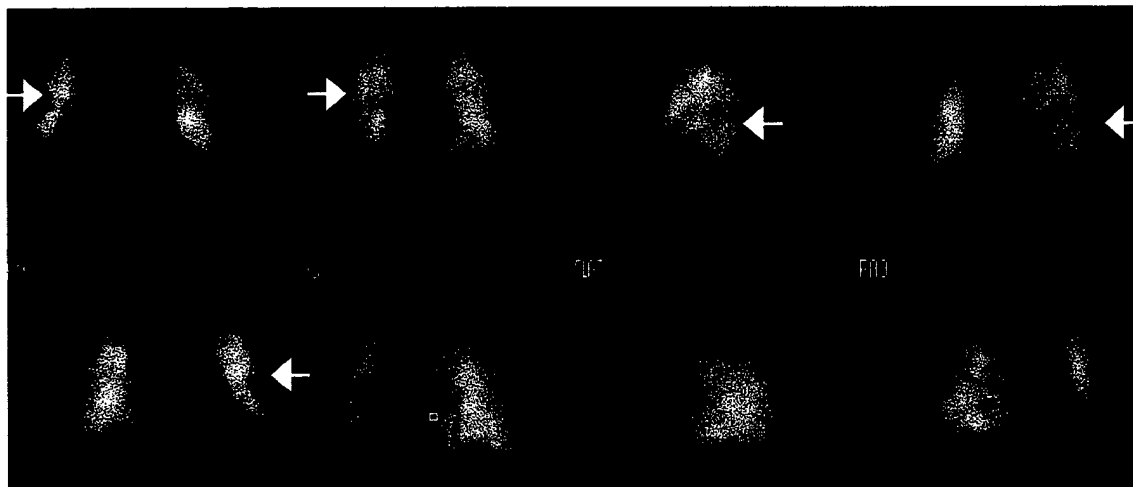


Figure 11. Undetected wedge shaped defect (lingula) located near white arrows.

5) In a few cases, large defects were classified as small or medium defects that lead to false negatives.

Based on the above study several improvements were made to the algorithm. These included methods for improved defect detection and classification, better separation of left and right lungs in oblique views, improved recognition of effects of heart in anterior views and diaphragms in lateral views. These enhancements decreased the number of false negative and false positive studies to one and zero, respectively. In comparison, physicians also had one false negative study. However, physicians classified 33% of the studies as intermediate while the software interpreted only 5% as intermediate. This software package is being marketed and the FDA application process is underway.

VQ scan interpretation has several limitations including a large number of intermediate probability scans, non-standardized interpretation schemes, and significant interobserver variability. We have developed a fully automated computer software which aids the nuclear medicine physician to interpret VQ scans and categorize the probability of PE. The final version of the software performed as well as the physician. In addition, the algorithm uses a standardized quantitative interpretation scheme, eliminates interobserver variability and greatly decreases the number of intermediate probability studies. By decreasing the number of intermediate studies, the program helps the referring physician and improves patient care by decreasing the need for further evaluation such as pulmonary angiogram.

In an identical manner, cardiac and bone scan interpretation programs were developed. The programs were based on an initial data-set and then the program was refined with additional data. Both of these programs' exhibited over 85% correct diagnosis on the limited data provided. More than 150 scans are required to develop and test the lung code. Less than that number were obtained for these other applications. However, in the pursuit of commercial markets we will continue to develop these programs and a host of diagnostic tools from this first tool.

## Why use a Pulse Coupled Neural Network

There are two main reasons for the success of the VQ scan interpretation software. First, the interpretation algorithm has successfully integrated knowledge of three nuclear medicine physicians. Secondly, the pulse coupled neural network is able to segment images with sufficient accuracy to permit the detection and quantification of defects. It is obvious that the accuracy of the interpretation system depends on the accuracy of the image segmentation system. Poor intensity contrast and noise appear to have less adverse effect on the performance of the PCNN than on the performance of human experts and other image segmentation methods. Perhaps, this is the primary reason for the decrease in the number of intermediate studies achieved by the software.

*Eckhorn* developed a pulse coupled neuron (PCN) is an artificial neuron designed to resemble biological neurons found in cat's visual cortex. Networks of pulse coupled neurons are known as pulse coupled neural networks (PCNN). *Ranganath* then developed two-dimensional, single layered and laterally connected pulse coupled neural networks are found suitable for image analysis, particularly for image segmentation and image smoothing. The PCNN is able to bridge small spatial gaps and minor intensity variations in spatial data or images. This property makes them highly desirable for the segmentation of digital images. A complete mathematical description of the PCN model and PCNN is beyond the scope of this paper. Therefore, a simple description of the structure PCN and operation of the PCNN is presented in the next section.

## Hardware Implementation of the Pulse Coupled Neural Network

A pulse coupled neuron consists of three major parts: a pulse generator, a threshold signal generator and a linking receptive field. Each neuron receives an external input  $X(t)$  and monotonically decaying linking inputs from all neighboring neurons that have fired. The initial strength of linking input from one neuron to another is inversely proportional to the square of the distance between them. The linking receptive field gathers linking inputs from individual neurons to produce the net linking input  $L(t)$ . The internal activity of the neuron denoted by  $U(t)$  is analogous to membrane potential of biological neuron. It is computed as the product of

$X(t)$  and  $(1+aL(t))$ , where  $a$  is a positive constant known as linking coefficient. In addition to  $U(t)$ , the pulse generator receives a second input known as threshold signal ( $T(t)$ ). The threshold signal may remain constant or decay monotonically depending on the application and mode of network operation. In any case, when the value of the internal activity is greater than the value of the threshold signal the neuron fires. Now, the pulse generator sends a narrow pulse on  $Y(t)$ , the neuron's output. As soon as the neuron fires, linking inputs are sent to its neighbors and the threshold signal is charged and clamped to a high value. This disables the neuron from further firing unless it is reset.

Now consider a simple network of two neurons in which only neuron  $N1$  is allowed to send linking input to neuron  $N2$  (Figure 2). Let  $X1$  and  $X2$  be the external inputs to  $N1$  and  $N2$ , respectively. Assume that  $X1 > X2$ . If  $T1$  and  $T2$  are both initialized to a value  $Tmax$  greater than  $X1$  and allowed to decay,  $N1$  will fire first and send a linking input to  $N2$ . Because of the linking input the value of  $U2$  increases from  $X2$  to  $X2(1+aL2)$ . If  $U2$  does not exceed  $T2$  then  $N2$  will fire at a later time. If  $U2$  exceeds  $T2$  then  $N2$  will fire with  $N1$ . Now,  $N1$  has captured  $N2$ . In a general network, the fire and capture process begins with a few naturally firing neurons and continues recursively. This process in which pulsing neurons cause other neurons to pulse by sending linking inputs in a recursive manner is known as the *capture phenomenon*.

The PCNN chip accepts input through a differential pair of photo-detectors that signal is amplified. The input intensity is multiplied with a linking input from a local neighborhood. The resultant signal is input to a comparator for the intensity thresholding. A D flip-flop stores the pixel state. These components are all integrated into a pulse coupled neuron (PCN). Each neuron is a pixel on the camera focal plane. The PCN circuit is shown in figure 12. These PCNs are tiled to form arrays. The CMOS Layout for that PCN pixel is 122  $\mu m$  in size and shown in Figure 6b. The layout for a single pixel is much larger than for a traditional camera because of the on-the-focal-plane processing that must occur. Optical sensitivity issues are easily resolved by altering the gain of the photodiode [Ampgain], and by mating the PCNN to a custom microlens array. This microlens array will be designed by SY Technology, Inc. and fabricated at the commercial company MemsOptical. MemsOptical is a Phase III partner for our innovative research and development efforts.



The schematic diagram illustrates the internal architecture of a 1-bit programmable logic device (PLD). It features a reference voltage divider (Ref, Vss) and a linear input (Lin) connected to a multiplier (X). The multiplier's output is fed into a current source (Vdd, Vss) and a summing circuit (Summing ckt) with a feedback resistor (R=40K). The summing circuit's output is compared by a comparator (Comparator). The comparator's output is connected to a D flip-flop (DFF Q) and various logic gates (AND, OR, XOR, NAND). The output of the DFF Q is labeled 'Col out'.

This is a high-contrast, black-and-white aerial photograph of a city grid, likely New York City. The image shows a dense arrangement of building footprints and street patterns. The right side of the image is heavily degraded with vertical streaks and noise, possibly from a scanning artifact or film damage. The overall image quality is poor, with significant noise and artifacts throughout.

A large, dense, black and white image showing a highly textured, possibly woven or knitted fabric. The texture is very fine and uniform across the entire surface. The image is framed by a thick black border, which is itself surrounded by a white border. The overall appearance is that of a high-contrast, close-up photograph of a textile material.

Figure 12. a) Pulse coupled neuron schematic. This neuron is one pixel. The lightning bolt arrow is the optical input. This input can be overridden in an electronic PCNN also under development. b) The L-Edit layout for the pixel/neuron. c) tiled 32x32 PCNN array.

25

**Table 2 PCNN Prototype Test Results**

Component	Comments
Phototransistor	Low dark current, alternatives with variable dynamic range under test
Multiplier	Good gain control over range of Beta = .8 to 1.2 volts – Need Higher Gain for some commercial applications
Amplifier	Good gain control over range of Amplifier gain = .8 to 1.2 volts
Current summer	Output range from 2.0 to 4.5 volts
Comparator	Switches normally with high speed
Multiplexer	Prevents multiple triggering of neuron as required
D-Flip-Flop	Stores neuron trigger state as required
Exclusive NOR	Functions normally
Output transistor	Drives resistive grid normally
Resistive grid	Observed Linking - Increase Linking Voltage

The prototypes were illuminated with various test images and the segmentation of the optical input was observed. In this case a light and dark pattern is imaged onto the array. The chip exhibited a staggered segmentation result, figure 13. This is due to interconnectivity noise that was not detected in the component by component test procedures. The source of the noise has been located. The test board and multiplexed signal currents were a source. In addition a new ground plane design has been submitted to improve the

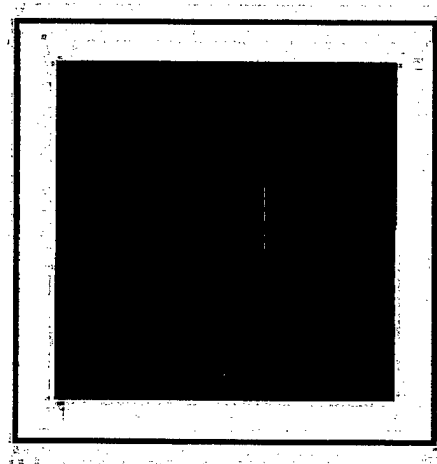


Figure 13. Segmented image with 1/2 of array illuminated

performance. The chip is due to be submitted at the end of May 1999 and should be received at SY Technology Inc. in 10 weeks.

## Recommendations

Among the outcomes of this research, the lung scan program was developed as a comprehensive computerized method of analyzing Xenon ventilation and perfusion scans for pulmonary embolism. This analysis aids in the detection and localization of unmatched pulmonary defects, which are indicators of pulmonary embolism. The lung scan program was developed to operate in a manner similar to the Cedars-Sinai quantitative thallium analysis program.

The lung scan program highlights the unmatched pulmonary defects as an overlay on the ventilation and perfusion imagery. First, the software program automatically processes each of the lung scan images. Then the software program locates and computes each lung's size. From each of the lung's shape and size, the perfusion and ventilation defects are located. The software program locates retained radioactivity in the three minute washout image. From this data the software program computes a probability of pulmonary embolism.

The user may accept this diagnosis if there are no mitigating defects on the Chest X Ray or contradicting evidence in the patient history. To date Chest X Ray findings are not included in the diagnostic criteria. The software relies on the physician running the program to take this X Ray data, and patient history into account when interpreting the graphical display.

Fully automated computer programs were demonstrated for a number of medical scan interpretation applications. The pulse coupled neural network used to segment images in defense and space applications was found to be suitable for the segmentation of digital medical scans. The clinical studies with actual patients, and software running in a medical hospital has shown that the software performs as well as the nuclear medicine physician. In addition, the algorithm, by using a standardized quantitative interpretation scheme, eliminates interobserver variability, greatly decreases the number of intermediate probability studies, and thereby improves patient outcomes.

Mapping the PCNN algorithm to an opto-electronic chip proved possible and results demonstrate the basic operation of the prototype. The integrated circuit has been fabricated a number of times and is susceptible to noise. This noise causes less than ideal segmentation results. The next generation chip has been modified to improve operating characteristics. Large array sizes will be available in the near future.

### References

1. The PIOPED Investigators. Value of the Ventilation/Perfusion Scan in Acute Pulmonary Embolism. *JAMA*, May23/30, 1990; 263: 2753-2759.
2. Sostman HD, Coleman RE, DeLong DM, Newman GE, Paine S. Evaluation of Revised Criteria for Ventilation-Perfusion Scintigraphy in Patients with Suspected Pulmonary Embolism. *Radiology* 1994; 193:103-107.
3. Gottschalk A, Juni JE, Sostman HD, Coleman RE, Thrall J, McKusick KA, Froelich JW, Alavi A. Ventilation-Perfusion Scintigraphy in the PIOPED study. Part I, Data Collection and Tabulation. *J Nucl Med* 1993;34:1109-1118.
4. Valdivia S, Banish MR, Ranganath HS, Christian PE, Datz FL. Computer Program developed for Clinical use Diagnoses Pulmonary Embolism and minimizes Intermediate Classifications. *J Nucl Med* 1997, 38:6P.
5. Eckhorn, R., Reitboeck, H. J., Arndt, M. and Dicke, P., "Feature linking via Synchronization among distributed assemblies: Simulation results from cat's visual cortex," *Neural Computation*, 2, 293-307, MIT, 1990.
6. Kuntimad, G., "Pulse coupled neural network for image processing," doctoral dissertation, Computer Science department, The University of Alabama in Huntsville, Huntsville, 1995.
7. Ranganath, H. S., and Kuntimad, G., "Image segmentation using pulse coupled neural networks", *Proc. IEEE International Conference on Neural Networks*, Orlando, FL., June 28 - July 2, 1994, vol.2, pp.1285-1290.
8. Germany, G. A., Parks, A. K., Ranganath, H. S., Elsen, R., Richards, P. G., Swift, W., Spann, J. F., Brittnacher, M., "Analysis of auroral morphology: Substorm precursor and onset on January 10, 1997", *Geophys. Res. Lett.*

9. Valdivia, S., Banish, M. R., Ranganath, H. S., Christian, P. E., and Datz, F. L., "Computer program developed for clinical use diagnoses pulmonary embolism and minimizes intermediate classifications," SNM 45th annual meeting 1998.
10. Banish, M, Clark R, Datz, FL, Christian, P." Automated interpretation of nuclear medicine scans for the diagnosis of pulmonary embolism" Proceedings of SPIE Advanced Imaging Technologies and Commercial Applications. Vol 2566, pg 16-25, San Diego, July 1995.

DISTRIBUTION LIST

AUL/LSE

Bldg 1405 - 600 Chennault Circle  
Maxwell AFB, AL 36112-6424

1 cy

DTIC/OCP

8725 John J. Kingman Rd, Suite 0944  
Ft Belvoir, VA 22060-6218

2 cys

AFSAA/SAI

1580 Air Force Pentagon  
Washington, DC 20330-1580

1 cy

AFRL/PSTL

Kirtland AFB, NM 87117-5776

2 cys

AFRL/PSTP

Kirtland AFB, NM 87117-5776

1 cy

SY Technology, Inc.

654 Discovery Drive  
Huntsville, AL 35806

1 cy

AFRL/DE/Dr. Charles B. Hogge

3550 Aberdeen S.E.  
Kirtland AFB, NM 87117-5776

1 cy

Official Record Copy

AFRL/DEBA/Judith Miller  
3550 Aberdeen S. E.

Kirtland AFB, NM 87117-5776

1 cy